Clinica Chimica Acta 490 (2019) 176–180

Contents lists available at ScienceDirect

Clinica Chimica Acta

journal homepage: www.elsevier.com/locate/cca

Real time detection of glutathionse in chemotherapy squamous-cell carcinoma cells of a fluorescent probe

Mengxing Qi[a,1], Meng Ma[c,1], Shengyun Huang[a], Dongsheng Zhang[a,*,2], Hongchen Liu[b,c,**,2]

[a] Department of Stomatology, Shandong Provincial Hospital Affiliated to Shandong University, Jinan 250021, China
[b] Institute of Stomatology, Chinese People's Liberation Army General Hospital, Beijing 100853, China
[c] Medical School, Nankai University, Tianjin 300071, China

ARTICLE INFO

Keywords:
GSH
Chemotherapy resistance
Real time
Fluorescent probe
Squamous-cell carcinoma

ABSTRACT

Glutathione (GSH) plays a key role in protecting damage induced by radiation and chemotherapy drugs. Current methods, which quantify GSH level changes by using cellular extraction or being based on redox homeostasis results, are unable to directly measure real time GSH level in live cells. In this article, we utilized a newly designed reversible fluorescent probe to measure GSH in living cells. The image of probe 1 can reveal intracellular GSH location and GSH level changes caused by different chemotherapy drugs in squamous-cell carcinoma cells. The results show that it is the first report with probe 1 that to quantify real-time GSH level changes in the cultured chemotherapy cancer cells and different changes in GSH level that may confer chemotherapy resistance.

1. Introduction

Glutathione (GSH) offers crucial antioxidant protection from reactive oxygen species (ROS) arising from radiotherapy and chemotherapy and GSH mediates resistance to these types of treatment [1,2]. Also, GSH is associated with diseases including cancer and malformations such as cleft palate [3–6].Reliable methods for measuring GSH will advance understanding of GSH-mediated detoxification mechanisms [7] as well as help diagnose potential disease at a molecular level [8–15]. Current methods, which quantify GSH level changes by using cellular extraction or being based on redox homeostasis results, are unable to directly measure real time GSH levels in living cells [16].Among various analytical methods available to measure GSH fluorescent molecular imaging is the most sensitive and simple [17–20] but few methods measure GSH in real time. Thus, we utilized a membrane-permeable fluorescent probe (Fig. 1) for imaging GSH in living cells.

Specifically, we measured GSH in the context of squamous-cell carcinoma (SCC), the most common carcinoma of the head and neck area [21] and its treatment, surgery plus radiation. The efficacy of chemotherapy for SCC is much poorer than other carcinomas [22].We tried to understand why chemotherapy for treating SCC is suboptimal and whether GSH may contribute to poor outcomes. We measured GSH in SCC cell line Cal-27 treated with different kinds of chemotherapy and used a confocal laser scanning microscope (CLSM) to visualize results.

2. Methods

2.1. Cell lines and culture

Given as a gift from Professor Wantao Chen (Department of Oral and Maxillofacial Surgery, Ninth People's Hospital, Shanghai Jiao Tong University School of Medicine, China),Cal-27 cells were grown in Dulbecco's Modified Eagle Medium (DMEM) (high glucose)(Hyclone) supplemented with 10% heat-inactivated bovine serum were maintained in an incubator at 37 °C with a 5% CO_2/air environment. When cells reached a period of logarithmic growth by cell counting, we treated them with the probe 1.

2.2. Fluorescent probe

Given as a gift from Professor Baocun Zhu (School of Resources and Environment, University of Jinan, Shandong Provincial Engineering Technology Research Center for Ecological Carbon Sink and Capture

* Corresponding author.
** Corresponding author at: Institute of Stomatology, Chinese People's Liberation Army General Hospital, Beijing 100853, China.
E-mail addresses: ds63zhang@sdu.edu.cn (D. Zhang), liu-hc301@hotmail.com (H. Liu).
[1] Authors share co-first authorship.
[2] Authors share co-corresponding authorship.

https://doi.org/10.1016/j.cca.2018.09.003
Received 16 May 2018; Received in revised form 29 August 2018; Accepted 3 September 2018
Available online 05 September 2018
0009-8981/

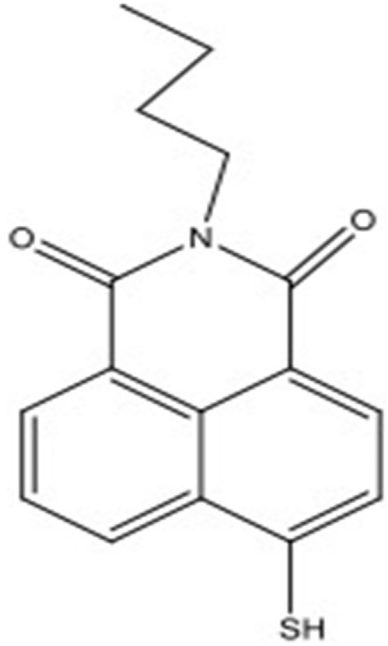

Fig. 1. Structure of probe 1.

Utilization, Jinan 250022, China),probe 1 was dissolved in DMSO (Sigma-aldrich, USA)for 1 mMol/mL as mother solution. Then Cal-27 cells are incubated with probe 1 (10 μMol) at 37 °C for 20 min.

2.3. Optical analyses

All optical images were performed at 37 °C, Cal-27 cells were cultured in 1 mL DMEM (high glucose) (Hyclone) supplemented with 10% heat-inactivated bovine serum in a glass culture dish.

2.4. Fluorescence imaging system

In this study, confocal laser scanning microscope (Zeiss LSM780, Carl Zeiss, Germany) was used. Blue fluorescence images were obtained using an excitation wavelength of 405 nm and a band- path (410–519 nm) emission filter, red fluorescence images were obtained using an excitation wavelength of 561 nm and a band- path (599–759 nm) emission filter.

2.5. Quantitative analysis

At each image, the fluorescence intensity of a region of interest (ROI) over was quantified by using ZEN2012 software.

2.6. Statistical methods

Data are means ± SD. Differences in actual outcomes between groups were calculated using a Student's *t*-test (*t*-test). All analyses were performed with the Statistical Package for the Social Sciences, version 12.0 (SPSS, Chicago, IL). A p value of 0.05 was set as the significant level.

3. Results

3.1. Location of the GSH

To confirm the biological relevance of our fluorescent probe, Cal-27 cells were incubated with probe 1 (10 μmol) and MitoTracker® Red CMXRos (Invitrogen, 10 μmol) to identify mitochondria at 37 °C for 20 min and noted that (Fig. 2), blue fluorescence was localized to cytoplasm and mitochondria whereas red fluorescence was apparent in mitochondria. Thus, the probe 1 could permeate live cells and react with resident GSH. The fluorescent intensity in Fig. 2 indicates that GSH was located in the cytoplasm and mitochondria. GSH distributes more in mitochondria, called GSH reservoir [23,24].

3.2. To explore the appropriate intensity of laser for continuous detection

We assessed probe stability by incubating it with live Cal-27 cells at 37 °C for 20 min. Fluorescent emission was observed and images were captured every 42.5 s by using the confocal laser scanning microscope (Zeiss LSM780, Carl Zeiss, Germany). Two laser intensities 0.5% and 1.5% (405 nm) were used to continuously observe fluorescent intensity changes for 5 min (Fig. 3). Fluorescent intensity was calculated as the mean fluorescent intensity of the image minus background by using ZEN2012 software (Carl Zeiss, Germany) and all experiments were conducted in triplicate. Data showed that (Fig. 4; Table 1) fluorescent intensity of the 0.5% intensity laser was stable and it showed that cells were not damaged. There was a statistically significant difference between the 0.5% and 1.5% intensity laser group treatments (Table 1) and fluorescent intensity of 1.5% intensity laser decreased gradually as time went on.

3.3. Detection of GSH changes with different chemotherapy drugs

We incubated the probe 1 (10 μmol) with Cal-27 cells at 37 °C for 20 min and acquired images under a 0.5% intensity laser every 42.5 s using a CLSM. Three groups of Cal-27 cells were respectively treated with different chemotherapy drugs, cisplatin (DDP) (3 mg/L), DDP (3 mg/L) + Five fluorouracil (5FU) (30 mg/L) and DDP (3 mg/L) + 5FU (30 mg/L) + Paclitaxel (3 mg/L), which are the three most common therapeutic schemes in head and neck carcinoma treatment [25]. Drug concentrations approximated maximum plasma concentrations of the patient to best simulate in vivo cancer cells' environment during chemotherapy [26,27]. All experiments were conducted in triplicate.

Fluorescent intensity was observed for 3 min (Fig. 5, 0–2.832 min) (Fig. 6 line A–B) to ensure the intensity was stable. Then three groups of chemotherapy drugs were separately added into three cell culture medium at the 3-minite time point (Fig. 5, 2.832 min) (Table 2 and Fig. 6, point B).After adding chemotherapy drugs, Cal-27 cells rapidly constricted and the fluorescence intensity increased to the top(Fig. 5, 3.54 min) (Table 2 and Fig. 6, point C).The fluorescence intensity at point C of group DDP + 5FU + Paclitaxel was significantly lower than the other two groups. Then Cal-27 cells began to diastole (Fig. 5, 3.54–4.957 min)(Fig. 6, line C–D). The constriction and diastole process (Fig. 6 line B–D) lasted for about 2 min.

From 4.957 min in Fig. 5 (Table 2 and Fig. 6, point D) the cells began a constriction process gradually. The line D–E in Fig. 6 of DDP group and DDP + 5FU group in Fig. 6 began to grow while the line D-E in Fig. 6 of DDP + 5FU + Paclitaxel group in Fig. 6 was still dropping. From 14.865 min in Fig. 5 (Table 2 and Fig. 6, point E) the fluorescence intensity became stable again. For the final GSH level (Fig. 5, 14.865–19.112 min) (Fig. 6, line E–F), DDP + 5FU + Paclitaxel group < DDP + 5FU group < DDP group. There were statistically significant differences among the three groups. At fifteenth minute the fluorescent intensity was not changed for the additional 5 min of observation.

4. Discussion

The resistance to chemotherapy and radiotherapy is the primary problem confronted in the treatment of SCC [28].The mechanism of GSH and ROS formation is the main reason for the resistance. Recent studies have proven that chemotherapy drugs can increase GSH level which is critical to the progression of apoptosis [29]. However it can be

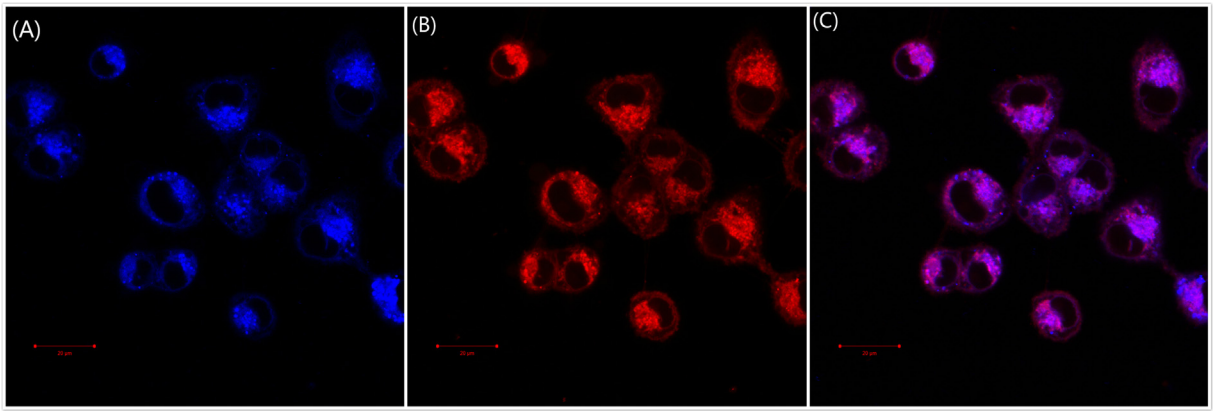

Fig. 2. Confocal laser scanning microscope images of probe 1 in cal-27 cells. (A) Blue channel fluorescence image of cal-27 cells incubated with probe 1 (10 μM) and MitoTracker® Red CMXRos(10 μM) (B) Red fluorescence image of cal-27 cells incubated with probe 1 (10 μM) and MitoTracker® Red CMXRos(10 μM) (C)Mix two channels fluorescence image of cal-27 incubated with probe 1 (10 μM) and MitoTracker® Red CMXRos (10 μM).

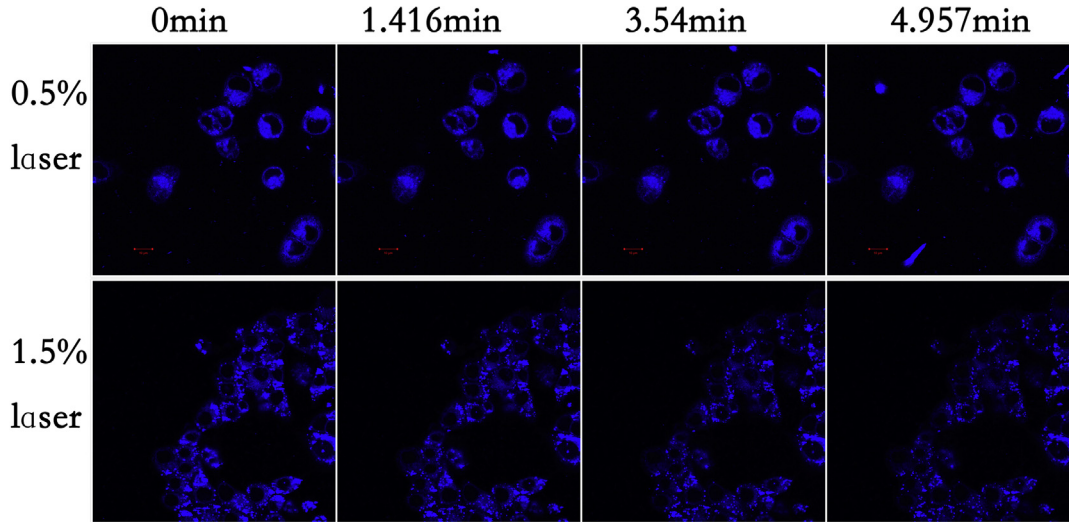

Fig. 3. Time series fluorescence image under 0.5% and 1.5% intensity laser.

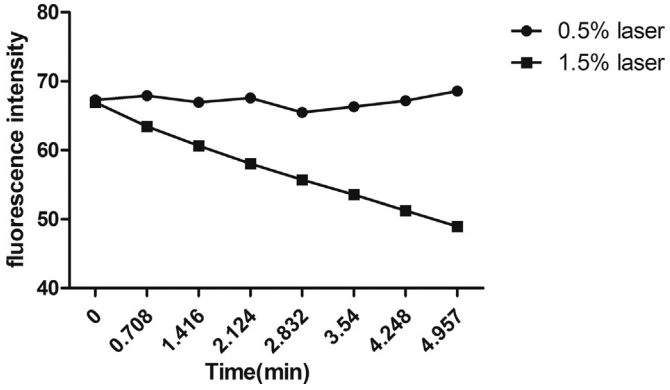

Fig. 4. Time series fluorescence intensity changes under 0.5% and 1.5% intensity laser.

prevented by the prohibition of GSH depletion [30]. From Fig. 2, we see that the concentration of GSH in mitochondria is much higher than the others, which is called GSH reservoir. Moreover, the main source of ROS is mitochondria and it depends on GSH to deal with ROS formation and protect cells.

Intense laser energy can produce ROS that damage cells. From Figs. 3, 4 and Table 1, GSH decreases to cope with the increasing ROS so as to protect the cells under high intensity laser. The common laser intensity is 40%–60% when using CLSM. In order to detect real time GSH changes for a long time, a low intensity laser should be chosen. We selected two very low intensities 0.5% and 1.5% and data (Fig. 4; Table 1) showed that fluorescent intensity of the 0.5% intensity laser was stable besides that of the 1.5% intensity laser decreased gradually as time went on. So a very low intensity laser is needed for continuous detection and should be tested when using CLSM.

We observed the dynamic reaction of the Cal-27 cells and GSH changes when chemotherapy drugs were added. Cal-27 cells rapidly

Table 1
Time series fluorescence intensity changes under o.5% and 1.5% laser.

Lazer intensity\time(min)	0	0.708	1.416	2.124	2.832	3.54	4.248	4.957
0.5% laser	67.268	67.927	66.960	67.567	65.474	66.331	67.174	68.576
1.5% laser	66.937	63.435	60.658	58.057	55.729	53.543	51.261	48.963
p	0.5628	0.0006	2.3E-06	1.3E-06	4.4E-08	8.7E-06	2.6E-07	5.2E-09

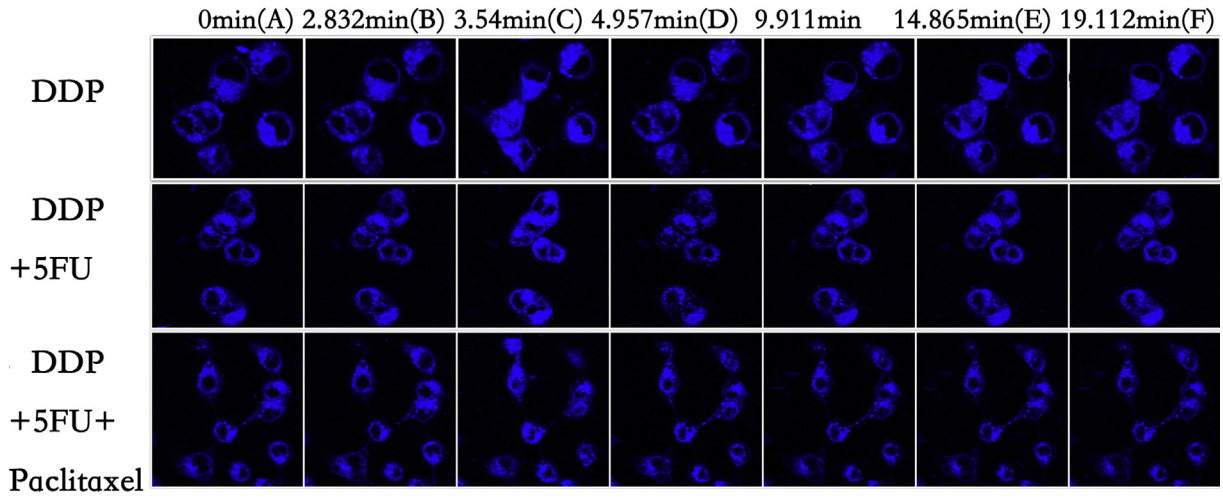

Fig. 5. Time series fluorescence image treated by DDP, DDP + 5FU and DDP + 5FU + Paclitaxel.

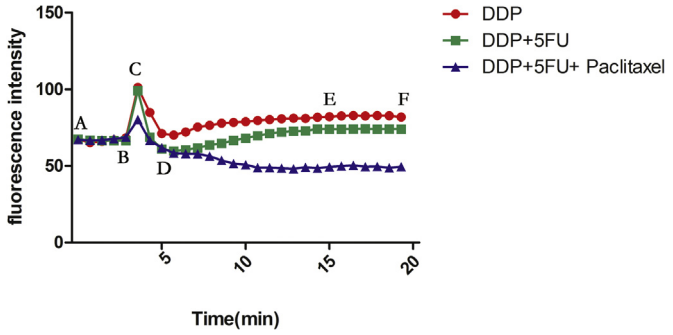

Fig. 6. Time series fluorescence intensity changes treated by 3 chemotherapy schemes. (The point A,B,C,D,E,F are the same as the point A,B,C,D,E,F in Table 2.)

constricted after adding chemotherapy drugs so as to reduce the contact area exposed to chemotherapy drugs and the fluorescence intensity increased to the top (Fig. 5, 3.54 min) (Table 2 and Fig. 6, point C).The fluorescence intensity at point C of group DDP + 5FU + Paclitaxel was significantly lower than the other two groups due to greater ROS production and greater GSH consumption. After constriction, Cal-27 cells began to diastole slowly (Fig. 5, 3.54–4.957 min) (Fig. 6, line C–D). Then, Cal-27 cells enlarged (Fig. 5, 4.957 min) (Table 2 and Fig. 6, point D) but they were smaller than their original size. The constriction and diastole process (Fig. 6 line B–D) lasted for about 2 min. In this process the resident GSH in cells was consumed to oppose the ROS induced by chemotherapy drugs. Obviously group DDP + 5FU + Paclitaxel consumed much more resident GSH than the other groups as more ROS production.

From 4.957 min in Fig. 5 (Table 2 and Fig. 6, point D) the cells began a second constriction process gradually, and from this point cells began to composite GSH using the amino acid from the environment (cell culture medium) to deal with ROS. So the line D–E in Fig. 6 of DDP group and DDP + 5FU group in Fig. 6 began to grow because of the newly synthesized GSH. But the line D-E in Fig. 6 of DDP + 5FU + Paclitaxel group in Fig. 6 was still dropping as Paclitaxel produced much more ROS, that was the reason why Paclitaxel was more available to kill cancer cells and reached much significant curative effect in clinical caner treatment. From 14.865 min in Fig. 5 (Table 2 and Fig. 6, point E) the fluorescence intensity became stable again as the producing GSH was balanced to the ROS induced by chemotherapy drugs, which was a continuous process. For the final GSH level (Fig. 5, 14.865–19.112 min) (Fig. 6, line E–F), DDP + 5FU + Paclitaxel group < DDP + 5FU group < DDP group. There were statistically significant differences among the three groups. High GSH protected cancer cells from chemotherapy-induced death and the final GSH level (Fig. 5, 14.865–19.112 min) (Fig. 6, line E–F) measured here was similar to in vivo GSH level for patient in chemotherapy. It took 12 min for Cal-27 cells to reach GSH equilibrium (Fig. 6 and Table 2, point E) after adding chemotherapy drugs.

Table 2
Time series fluorescence intensity changes treated by 3 chemotherapy scheme.

Chemotherapy scheme\time(min)	0 (A)	0.708	1.416	2.124	2.832 (B)	3.54 (C)	4.248	4.957 (D)	5.665	6.372	7.081	7.787	8.495	9.203
DDP	67.352	65.266	66.12	66.961	68.358	101.324	84.878	71.238	70.141	72.161	75.38	76.562	77.98	78.482
DDP + 5FU	67.431	66.784	66.515	66.526	66.546	99.24	68.842	61.017	59.85	60.569	61.867	63.646	64.802	66.635
DDP + 5FU + Paclitaxel	67.141	66.687	66.974	67.659	68.76	80.314	66.734	61.946	58.447	58.035	57.89	56.469	53.71	51.548
p1	0.5516	0.1963	0.6986	0.6949	0.0602	0.0062	1.3E-05	8.5E-06	2.8E-05	8.5E-06	2.1E-06	2.6E-06	5.9E-06	4.0E-07
p2	0.6890	0.8951	0.6632	0.1330	0.0006	3.7E-07	0.0332	0.1814	0.0359	0.0027	0.0001	4.3E-06	1.4E-05	2.1E-07

Chemotherapy scheme\time (min)	9.911	10.619	11.327	12.035	12.743	13.449	14.157	14.865 (E)	15.573	16.28	16.988	17.696	18.404	19.112 (F)
DDP	78.881	79.668	80.347	80.819	81.185	81.042	81.811	82.137	82.673	82.947	82.677	82.961	82.802	81.96
DDP + 5FU	68.224	69.782	71.22	72.238	72.687	72.991	74.185	74.056	74.044	74.217	74.365	74.044	74.178	74.026
DDP + 5FU + Paclitaxel	50.762	48.903	48.998	48.579	48.153	49.135	48.514	49.411	49.998	50.395	49.501	49.685	48.769	49.602
p1	1.0E-06	8.1E-06	9.7E-06	4.9E-06	1.1E-05	3.1E-06	1.3E-05	7.1E-05	3.5E-05	2.8E-06	3.3E-05	5.2E-05	6.5E-05	1.7E-05
p2	4.1E-08	5.1E-07	6.6E-07	1.4E-07	2.5E-07	4.2E-08	5.2E-08	3.4E-06	5.3E-08	3.5E-07	6.6E-07	5.1E-07	3.2E-07	1.1E-07

The A,B,C,D,E,F are the same as the point A,B,C,D,E,F in Fig. 5.
p1 means the statistical differences between DDP and DDP + 5FU, p2 means the statistical differences between DDP + 5FU and DDP + 5FU + Paclitaxel.

5. Conclusion

In summary, the results show that it is the first report with probe 1 that to quantifying real-time GSH level changes in cultured chemotherapy cancer cells. The results of this study demonstrate the feasibility of probe 1 imaging in detecting GSH in SCC cells. The probe 1 is cell-permeable and can monitor specific cellular locations of GSH. Also, fluorescent intensity is stable when cells are incubated with the probe 1 using a 0.5% intensity laser (405 nm) under the confocal laser scanning microscopy. The probe 1 can be used to measure GSH changes in living cancer cells during different chemotherapy, which may confer chemotherapy resistance.

Author contributions

M.Q and M.M conceived the experiments, H.S data analysis. D.Z and H.L project planning, conducted the experiments.

Competing financial interests

The authors declare no competing financial interests.

Acknowledgment

We gratefully acknowledge the financial support by Primary Research & Development Plan of Shandong Province (grant numbers 2016GSF201174).

Our Laser confocal scanning imaging work (Zeiss LSM780) was performed at The Microscopy Characterization Facility, Shandong University.

References

[1] J.K. Kwee, A paradoxical chemoresistance and tumor suppressive role of antioxidant in solid cancer cells: a strange case of Dr. Jekyll and Mr. Hyde, BioMed Res. Int. 2014 (2014) 209845.
[2] Y. Ohta, K. Yashiro, K. Ohashi, Y. Horikoshi, C. Kusumoto, T. Matsura, Compound 48/80, a mast cell degranulator, causes oxidative damage by enhancing vitamin C synthesis via reduced glutathione depletion and lipid peroxidation through neutrophil infiltration in rat livers, J. Clin. Biochem. Nutr. 60 (2017) 187–198.
[3] X.D. Zhang, S.K. Gillespie, J.M. Borrow, P. Hersey, The histone deacetylase inhibitor suberic bishydroxamate: a potential sensitizer of melanoma to TNF-related apoptosis-inducing ligand (TRAIL) induced apoptosis, Biochem. Pharmacol. 66 (2003) 1537–1545.
[4] S.J. Korsmeyer, M.C. Wei, M. Saito, S. Weiler, K.J. Oh, P.H. Schlesinger, Pro-apoptotic cascade activates BID, which oligomerizes BAK or BAX into pores that result in the release of cytochrome c, Cell Death Differ. 7 (2000) 1166–1173.
[5] J. Adams, The development of proteasome inhibitors as anticancer drugs, Cancer Cell 5 (2004) 417–421.
[6] J.R. Liddell, A.R. White, Nexus between mitochondrial function, iron, copper and glutathione in Parkinson's disease, Neurochem. Int. (2017).
[7] B. Kalyanaraman, V. Darley-Usmar, K.J. Davies, et al., Measuring reactive oxygen and nitrogen species with fluorescent probes: challenges and limitations, Free Radic. Biol. Med. 52 (2012) 1–6.
[8] C.C. Yeh, M.F. Hou, S.H. Wu, et al., A study of glutathione status in the blood and tissues of patients with breast cancer, Cell Biochem. Funct. 24 (2006) 555–559.
[9] J. Shao, H. Sun, H. Guo, et al., A highly selective red-emitting FRET fluorescent molecular probe derived from BODIPY for the detection of cysteine and homocysteine: an experimental and theoretical study, Chem. Sci. 3 (2012) 1049–1061.
[10] S.U. Khan, I. Mahjabeen, F.A. Malik, M.A. Kayani, Prognostic significance of altered blood and tissue glutathione levels in head and neck squamous cell carcinoma cases, Asian Pacific J. Cancer Prevent. 15 (2014) 7603–7609.
[11] S. Gurudath, K. Ganapathy, A. Pai, S. Ballal, A. Ml, Estimation of superoxide dismutase and glutathione peroxidase in oral submucous fibrosis, oral leukoplakia and oral cancer–a comparative study, Asian Pacific J. Cancer Prevent. 13 (2012) 4409–4412.
[12] Z. Guo, S.W. Nam, S. Park, J. Yoon, A highly selective ratiometric near-infrared fluorescent cyanine sensor for cysteine with remarkable shift and its application in bioimaging, Chem. Sci. 3 (2012) 2760–2765.
[13] N. Fu, D. Su, J.R. Cort, et al., Synthesis and application of an environmentally insensitive Cy3-based arsenical fluorescent probe to identify adaptive microbial responses involving proximal dithiol oxidation, J. Am. Chem. Soc. 135 (2013) 3567–3575.
[14] T. Dalton, H.A. Shertzer, Regulation of gene expression by reactive oxygen, Ann. Rev. Pharmacol. Toxicol. 39 (1999) 67–101.
[15] E.H. Cheteh, M. Augsten, H. Rundqvist, et al., Human cancer-associated fibroblasts enhance glutathione levels and antagonize drug-induced prostate cancer cell death, Cell Death Dis. 8 (2017) e2848.
[16] T. Lorincz, A. Szarka, The determination of hepatic glutathione at tissue and subcellular level, J. Pharmacol. Toxicol. Methods 88 (2017) 32–39.
[17] L. Zhang, B. Ling, L. Wang, H. Chen, A near-infrared luminescent Mn2+ −doped NaYF4:Yb,Tm/Fe3+ upconversion nanoparticles redox reaction system for the detection of GSH/Cys/AA, Talanta 172 (2017) 95–101.
[18] L.Y. Niu, Y.S. Guan, Y.Z. Chen, L.Z. Wu, C.H. Tung, Q.Z. Yang, BODIPY-based ratiometric fluorescent sensor for highly selective detection of glutathione over cysteine and homocysteine, J. Am. Chem. Soc. 134 (2012) 18928.
[19] Y. Guo, X. Yang, L. Hakuna, et al., A fast response highly selective probe for the detection of glutathione in human blood plasma, Sensors 12 (2012) 5940–5950.
[20] N. Shao, J. Jin, H. Wang, et al., Design of bis-spiropyran ligands as dipolar molecule receptors and application to in vivo glutathione fluorescent probes, J. Am. Chem. Soc. 132 (2010) 725–736.
[21] L.A. Torre, F. Bray, R.L. Siegel, J. Ferlay, J. Lortet-Tieulent, A. Jemal, Global cancer statistics, 2012, CA Cancer J. Clin. 65 (2015) 87–108.
[22] K.K. Chan, A.M. Glenny, J.C. Weldon, S. Furness, H.V. Worthington, H. Wakeford, Interventions for the treatment of oral and oropharyngeal cancers: targeted therapy and immunotherapy, The Cochrane Database of Systematic Reviews, 2015 (Cd010341).
[23] G. Calabrese, B. Morgan, J. Riemer, Mitochondrial glutathione: regulation and functions, Antioxidants Redox Signal. (2017).
[24] M. Marí, A. Morales, A. Colell, C. Garcíaruiz, N. Kaplowitz, J.C. Fernándezcheca, Mitochondrial glutathione: features, regulation and role in disease, Biochim. Biophys. Acta 1830 (2013) 3317.
[25] C.H. Hsieh, M.L. Hou, M.H. Chiang, et al., Head and neck irradiation modulates pharmacokinetics of 5-fluorouracil and cisplatin, J. Transl. Med. 11 (2013) 231.
[26] R. Chen, J. Li, W.W. Hu, M.L. Wang, S.L. Zou, L.Y. Miao, Circadian variability of pharmacokinetics of cisplatin in patients with non-small-cell lung carcinoma: analysis with the NONMEM program, Cancer Chemother. Pharmacol. 72 (2013) 1111.
[27] B.C. Kuenen, L. Rosen, E.F. Smit, B.C. Kuenen, et al., Dose-finding and pharmacokinetic study of cisplatin, gemcitabine, and SU5416 in patients with solid tumors, J. Clin. Oncol. 20 (2002) 1657–1667.
[28] R.H. Engel, A.M. Evens, Oxidative stress and apoptosis: a new treatment paradigm in cancer, Front. Biosci. A J. Virtual Library 11 (2006) 300.
[29] M. Landriscina, F. Maddalena, G. Laudiero, F. Esposito, Adaptation to oxidative stress, chemoresistance, and cell survival, Antioxid. Redox Signal. 11 (2009) 2701.
[30] R. Franco, J.A. Cidlowski, Apoptosis and glutathione: beyond an antioxidant, Cell Death Different. 16 (2009) 1303–1314.